PFC/JA-95-44

# Comparison of Detached and Radiative Divertor Operation in Alcator C-Mod

J.A. Goetz, C. Kurz,[1] B. LaBombard, B. Lipschultz,
A. Niemczewski,[2] G.M. McCracken, J.L. Terry, R.L. Boivin,
F. Bombarda,[3] P. Bonoli, C. Fiore, S. Golovato, R. Granetz,
M. Greenwald, S. Horne, A. Hubbard, I. Hutchinson, J. Irby,
E. Marmar, M. Porkolab, J. Rice, J. Snipes, Y. Takase,
R. Watterson, B. Welch,[4] S. Wolfe, C. Christensen,
D. Garnier, D. Jablonski, D. Lo, D. Lumma, M. May,[5]
A. Mazurenko, R. Nachtrieb, P. O'Shea, J. Reardon, J. Rost,
J. Schachter, J. Sorci, P. Stek, M. Umansky, Y. Wang

November, 1995

[1]Present address, University of California at San Diego, San Diego, CA.
[2]Present address, McKinsey & Company, Inc., London SW1Y 4UH, United Kingdom.
[3]Associazone EURATOM-ENEA, Frascati, Italy.
[4]Institute for Plasma Research, University of Maryland, College Park, MD.
[5]Department of Physics, The Johns Hopkins University, Baltimore, MD.

Submitted to Physics of Plasmas.

This work was supported by the U. S. Department of Energy Contract No. DE-AC02-78ET51013. Reproduction, translation, publication, use and disposal, in whole or in part by or for the United States government is permitted.

**Comparison of detached and radiative divertor operation in Alcator C-Mod**

J.A. Goetz, C. Kurz,[a] B. LaBombard, B. Lipschultz, A. Niemczewski,[b] G.M. McCracken, J.L. Terry, R.L. Boivin, F. Bombarda,[c] P. Bonoli, C. Fiore, S. Golovato, R. Granetz, M. Greenwald, S. Horne, A. Hubbard, I. Hutchinson, J. Irby, E. Marmar, M. Porkolab, J. Rice, J. Snipes, Y. Takase, R. Watterson, B. Welch,[d] S. Wolfe, C. Christensen, D. Garnier, D. Jablonski, D. Lo, D. Lumma, M. May,[e] A. Mazurenko, R. Nachtrieb, P. O'Shea, J. Reardon, J. Rost, J. Schachter, J. Sorci, P. Stek, M. Umansky, and Y. Wang

*Plasma Fusion Center, Massachusetts Institute of Technology, Cambridge, MA 02139, USA*

The divertor of the Alcator C-Mod tokamak routinely radiates a large fraction of the power entering the scrape-off layer. This dissipative divertor operation occurs whether the divertor is detached or not, and large volumetric radiative emissivities, up to 60 MW-m$^{-3}$ in ICRF-heated discharges, have been measured using bolometer arrays. An analysis of both ohmic and ICRF-heated discharges has demonstrated some of the relative merits of detached divertor operation versus high-recycling divertor operation. An advantage of detached divertor operation is that the power flux to the divertor plates is decreased even further than its already low value. Some disadvantages are that volumetric losses outside the separatrix in the divertor region are decreased, the neutral compression ratio is decreased, and the penetration efficiency of impurities increases.

[a] Present address, University of California at San Diego, San Diego, CA
[b] Present address, McKinsey & Company, Inc., London SW1Y 4UH, United Kingdom
[c] Associazone EURATOM-ENEA, Frascati, Italy
[d] Institute for Plasma Research, University of Maryland, College Park, MD 20742
[e] Department of Physics, The Johns Hopkins University, Baltimore, MD 21218

## I. INTRODUCTION

The current plan for ITER operation specifies that 150 MW flow across the separatrix into the scrape-off layer ($P_{SOL}$).[1] To reduce the heat loads on the divertor plates to technically feasible levels ( ~ 5 MW-m$^{-2}$ ) the ITER divertor specification then requires that the power flowing to the divertor plates is $\leq$ 50 MW ( 0.33 x $P_{SOL}$ ) and that divertor volumetric losses are $\geq$ 100 MW ( 0.67 x $P_{SOL}$ ). This must be done while maintaining a high density ($\bar{n}_e \geq \bar{n}_{Greenwald}$) and clean core plasma (central $Z_{eff} \leq 1.6$). Large volumetric losses are thus required in the divertor region to dissipate this power before it reaches the divertor plates and redistribute it over the surrounding first-wall. It is also desirable to minimize the detrimental effect of impurities on the core plasma. Therefore, impurities must be confined to the divertor with minimal concentrations in the core and scrape-off layer (SOL) plasma. This preferential compression of impurities would also aid in pumping helium born in the core plasma. It remains to be demonstrated that all these conditions can be achieved simultaneously.

At present, there are two methods for high power dissipation in the divertor region; operating the device with either a high-recycling or a detached divertor. In either scenario, the volumetric power losses in the divertor can be high. However, it appears that a number of characteristics of these two regimes are different. In particular, the spatial distribution of the radiating zones and the energy transport can be markedly different. In order to determine the viability of these two dissipative divertor regimes for a fusion reactor, it is necessary to explore their operational characteristics. Furthermore, the underlying physics mechanisms need to be identified in order to extrapolate such results to fusion reactor conditions.

Experiments to address these questions have been carried out in Alcator C-Mod.[2] The divertor geometry and the diagnostics used in these studies are described in Section II. Dissipative divertor operation is defined in Section III. Characterization

of the volumetric losses in the divertor region together with the identification of the primary radiating species is presented in Section IV. The advantages and disadvantages of detached versus high-recycling divertor operation are discussed in Section V.

## II. EXPERIMENT DESCRIPTION

Alcator C-Mod is a compact, high field tokamak with a "vertical-plate" divertor geometry. It operates routinely with a dissipative divertor, *i.e.*, in either the high-recycling or the detached divertor regime. Parallel heat flux in the scrape-off layer can approach that predicted for ITER ($q_{||}^{SOL} \leq 0.5$ GW-m$^{-2}$). The density in the divertor region can be greater than 1 x $10^{21}$ m$^{-3}$, approximately that predicted for ITER, thus enhancing the radiative capabilities of the divertor. The divertor plates and first-wall are composed of molybdenum with some carbon contamination. The central $Z_{eff}$ remains low even with this all metal design.

Experimental data reported here were obtained from 5.3 Tesla, lower single-null deuterium discharges utilizing ICRF (ion cyclotron range of frequencies) heating at the second harmonic of deuterium. More specific details of the design, operational capabilities and diagnostics of Alcator C-Mod can be found elsewhere.[2] The relevant details of the divertor geometry used for these experiments can be seen in Figure 1a. Shown are the separatrix and open and closed flux surfaces for a standard "vertical-plate" discharge.

The primary diagnostics for measuring characteristics of these dissipative divertor plasmas are Langmuir probes, bolometers, and ionization gauges located in the divertor region. The Langmuir probes directly measure electron temperature and electron density at the divertor plate and in the scrape-off layer outside of the divertor (also called upstream).[3] There are probes embedded in both the inner and outer divertor plates (see Figure 1a). The current collecting area of these domed probes

extends 0.5 mm beyond the surface of divertor plate to avoid the complexities of flush-mounted probes.[4] A reciprocating probe head equipped with four probe tips can be inserted into the SOL. This probe head can sample plasma up to the last-closed-flux-surface ( LCFS ) and is capable of being inserted up to three times per discharge. The EFIT[5] magnetics code is used to map the coordinates of the probes embedded in the divertor plates and the position of the reciprocating probe to the flux coordinate at the midplane. This mapping procedure allows comparison of the plasma conditions at the divertor plate and in the SOL upstream from the divertor.

The bolometer systems are used to determine the local radiation emissivity and the total radiated power of the plasma (photons plus neutral particles). Each bolometer detector consists of a blackened gold foil absorber separated by an insulating foil from gold meander resistors.[6] The foils absorb neutral particles and radiation from visible through x-ray energies. The layout of the bolometers in the Alcator C-Mod divertor is shown in Figure 1b. There are twelve collimated detectors that view the divertor region. Tomographic inversion of the chordal data to obtain local emissivities is routinely performed. The calculation is done, assuming axisymmetry, on a grid of 2 cm square pixels that span the divertor region in the poloidal plane. A non-negative constraint and spatial smoothing are used in the inversion algorithm.[7] For the purposes of power accounting, this divertor radiation, $P_{rad}^{div}$, is split into two parts, $P_{rad}^{div,in}$ = divertor radiation from inside the LCFS and $P_{rad}^{div,out}$ = divertor radiation from outside the LCFS. Radiation measurements in the main plasma are made with a toroidally-viewing array consisting of 24 detectors with 2 cm radial resolution.

Neutral gas pressures in the private flux zone of the divertor are measured with two independent gauges. There is a Baratron gauge located in a vertical port and an *in situ* linear ionization gauge located behind the outer divertor (see Figure 1a).[8] The neutral pressure on the midplane of the tokamak is measured with a standard

ionization gauge on one of the horizontal ports.

## III. CHARACTERISTICS OF DISSIPATIVE DIVERTOR OPERATION

The Alcator C-Mod divertor and SOL can be characterized by three distinct transport regimes.[9] These regimes are (1) sheath-limited, where the electron temperature and pressure measured at the divertor plate are equal to that measured in the SOL outside of the divertor (upstream), (2) high-recycling divertor, where the electron pressure is constant on a flux surface but large temperature and density gradients exist between the divertor plate and upstream, and (3) detached divertor, where large gradients in both the electron temperature and pressure exist between the divertor plate and upstream. The high-recycling and detached divertor regimes are dissipative divertor regimes in the sense that large fractions of the SOL power are radiated and it is these regimes that will be discussed in this paper.

Figure 2 displays the plasma profiles at the outer divertor plate and upstream from the divertor in the high-recycling and detached divertor regimes. On flux surfaces which are detached, the ratio of the upstream pressure to that in the divertor has been measured to be as high as 100. A necessary condition for detachment of a particular flux surface (shaded region in Figure 2) is that the electron temperature is below 5-6eV. This is consistent with the model that assumes ion-neutral interactions, *i.e.* charge-exchange, are important in removing momentum (causing a loss in pressure).[10] Also noteworthy is the fact that the Alcator C-Mod divertor plasma detaches at lower densities, relative to the Greenwald limit,[11] than other tokamaks.[12] One possible factor in determining this limit is the "vertical-plate" geometry of the divertor (see Figure 1).

The plasma discharge shown in Figure 3 shows a number of characteristics of an Alcator C-Mod dissipative divertor. The plasma current, constant at 0.8 MA, and the line-averaged central density, ramping from 1.0 to 2.4 x $10^{20}$ $m^{-3}$, are shown in

Figures 3a and 3b respectively. The total input power (solid line ) and the ICRF power (dashed line) are plotted in Figure 3c. The divertor plasma is in the high-recycling regime from 0.5 until 0.62 sec after which the divertor plasma begins to detach from the plates. This is indicated by a precipitous drop in electron pressure at the divertor plate (shown in Figure 3d). Throughout this time the divertor remains dissipative as ≥ 70% of the power flowing in the SOL ($P_{SOL}$) is radiated in the divertor region (Figure 3e). After the divertor detaches, $P_{rad}^{div} / P_{SOL}$ is nearly unity in this ohmic phase.

Starting at 0.7 sec, 2 MW of ICRF heating power (falling to 1 MW after 0.95 sec) is applied to the main plasma. Even with this increased input power, the divertor is dissipative, with $P_{rad}^{div} \geq 0.5 \times P_{SOL}$. The additional heating power increases the amount of power flowing into the SOL and the divertor plasma reattaches to the plates at 0.71 sec, *i.e.*, it returns to the high-recycling state. Note the dramatic increase in the electron pressure measured at the plate.

From 0.65 to 0.95 sec methane is puffed into the SOL to enhance the radiative losses there. This causes the divertor plasma to detach once again at 0.82 sec as indicated by the drop in electron pressure at the plate. Figure 3g shows the buildup of carbon in the divertor and the movement of the carbon radiation from the inner divertor (solid line) to the X-point (dashed line) after this detachment. This measurement has a time response of 45 msec. It is important to note that the central $Z_{eff}$ remains low (≤1.6) throughout the discharge even with ICRF-heating and methane puffing (see Figure 3f).

## IV. RADIATION MEASUREMENTS

Tomographic analysis of divertor bolometer array measurements yields the magnitude and distribution of the divertor volumetric loss emissivities. During high-recycling operation, the largest emissivity is located near the inner divertor (see Figure 4a). There is also significant emissivity spread along the outer divertor leg of the

separatrix. For this ohmic plasma, the peak in the emissivity has a value of $\leq$ 30 MW-$m^{-3}$. During a discharge, such as that depicted in Figure 3, with $\geq$ 2 MW of ICRF power added, the peak in the emissivity reaches a value of 60 MW-$m^{-3}$ with large regions having emissivities of $\geq$ 10 MW-$m^{-3}$. The largest emissivity is located on the inboard side only when the ion $\nabla B$ drift is directed toward the divertor. If the ion $\nabla B$ drift is directed away from the divertor the largest emissivity is located near the outer divertor plate.[13] For the remainder of this discussion, only results with the ion $\nabla B$ drift directed toward the divertor are presented.

As the divertor plasma becomes detached, the peak in the divertor emissivity moves inside the LCFS near the X-point (see Figure 4b). This movement can be rapid ( $\leq$ 10 msec ) or gradual ( $\geq$ 100 msec ) depending on how quickly the temperature in the divertor is evolving. It is well correlated with the decrease in the ion saturation current collected by probes embedded in the divertor plates. The peak values of the emissivity are very similar to those measured in the high-recycling divertor regime. When the divertor detaches, the total power losses inside the separatrix ($P_{rad}^{inLCFS} = P_{rad}^{div,in} + P_{rad}^{main}$ = divertor radiation from inside the LCFS plus main plasma radiation) become much larger than those in the divertor region outside the separatrix due to the spatial movement of the divertor volumetric losses and a slight increase in the main plasma radiated power. Also, the ratio of $P_{rad}^{div,out}$ to $P_{rad}^{div,in}$ changes from a value of about three to about one as the divertor plasma goes from the high-recycling to the detached divertor regime.

The location of the ionization and radiation zones are different and indicate that in detached divertor plasmas, the low temperature region extends far from the divertor plates. Figures 4b and 4c are contour plots of volumetric emissivity obtained from bolometer measurements and $D_\alpha$ emissivity obtained from tomography performed on $D_\alpha$ array measurements,[14] respectively, during a detached divertor discharge (time

slice = 0.68 sec from Figure 3). The ionization zone (close to where the $D_\alpha$ emissivity is a maximum, Figure 4c) and the radiation zone (where the volumetric emissivity is a maximum, Figure 4b) are readily identifiable and clearly different. Note that the two zones overlap near the outer divertor at the point where the divertor geometry changes from "vertical-plate" to "flat-plate" (nearly horizontal plate). This correlates with the radial extent of the detached flux surfaces as indicated by the divertor probes (see Figure 2).

Studies have been undertaken to determine the composition of the volumetric emissivity in the X-point region. An extreme-ultraviolet ( XUV ) spectrograph[15] and a visible spectrograph have been used to survey the radiation coming from the divertor region. For these studies, the X-point had been shifted to larger major radius and up vertically to be in the field-of-view of the XUV spectrograph. These studies show that the total radiation emissivity is dominated by the XUV radiation.

For non-dissipative divertor plasmas with low central density ($\bar{n}_e^{main} \sim 1 \times 10^{20}$ $m^{-3}$), the significant contributors to the observed radiation in the XUV wavelength range of 60 - 1160 Å are argon, fluorine, carbon, and oxygen (see Table I). Argon is normally puffed in trace amounts to perform core ion temperature measurements while the other three are intrinsic impurities. Since most of the deuterium line emission is not in the observed spectral region, the total contribution of deuterium to the power is calculated from the observed brightness of the $D_{Ly\beta}$ line. At these lower densities $D^0$ is not a major radiator. As the central density is raised, the divertor plasma enters the dissipative divertor regime. Argon, fluorine, carbon, and oxygen remain significant radiators (see Table I). In this regime the contributions of $D^0$ line radiation and continuum emission (assumed to be bremsstrahlung) become significant in the power balance. In all cases, molybdenum is a negligible contributor to the XUV and visible radiated power.

In addition to determining the sources of the radiation in the divertor, it is of

interest to compare the measured radiation intensities with the intensities measured by the bolometers. This comparison was made by summing all of the emission in the 60 - 1160Å wavelength range (continuum included) as measured along a spectrograph viewing chord and comparing the resulting total brightness to that measured by a bolometer which views along essentially the same (but toroidally displaced) chord. The results of this comparison are displayed in Figure 5. Also included in this figure is the contribution from all the deuterium lines, as calculated from the $D_{Ly\beta}$ line brightness (the contribution from the visible spectrum between 4000 and 9000Å is negligible). The bolometer measures all the radiation emitted from the plasma plus the power removed from the plasma by charge-exchange neutrals, while the XUV and visible measurements miss the radiation between 1160 Å and 4000 Å. Nonetheless the measurements agree at low density ($t < 0.65$ s) within the absolute calibration uncertainties of the diagnostics. However, in the dissipative divertor regime ($t > 0.65$ s), the two time histories are strikingly different. The bolometer brightness nearly doubles, while the total detected XUV radiation brightness is essentially unchanged.

This discrepancy in the temporal behavior of the bolometer and XUV total brightness points to charge-exchange neutrals as being an important loss mechanism in the high density, dissipative divertor. The $D^0$ radiative loss and charge-exchange loss are intimately related, since each is proportional to $n_0 n_{e,i}$ as long as both the neutrals and the radiation escape the plasma. A simple estimate of the ratio of these losses can be made by comparing the relevant rate coefficients. This exercise yields a ratio of charge exchange power to total deuterium radiation power that rises strongly (from a value of about one) at temperatures of $< 3$ eV. Thus the time history differences seen in Figure 5 suggest that (1) the charge-exchange contribution to the divertor power loss is significant in the dissipative divertor regimes on Alcator C-Mod, and (2) this loss occurs in a region of low ($< 3$ eV) temperature.

## V. HIGH-RECYCLING VS. DETACHED DIVERTOR

During high-recycling divertor operation, total power losses in the relatively small divertor region can be equal to the total power losses inside the separatrix. This is because the local emissivities in the divertor region are at least twenty times greater than those in the main plasma. The ratio $P_{rad}^{div,out} / P_{rad}^{inLCFS}$ has been measured to be as high as 1.8. This ratio is an indication of how efficiently the divertor volume is being used as a radiating region. When the divertor plasma detaches, the ratio becomes much smaller (see Figure 6). This is a result of the peak in the divertor volumetric emissivity moving inside the LCFS near the X-point as well as a slight increase in the radiated power in the main plasma. Under detached divertor conditions, the divertor volume is no longer being used as effectively as a radiating region as it was under high-recycling divertor conditions.

The penetration efficiency of impurities is observed to increase when the divertor plasma is detached from the plates. This is illustrated in Figure 7. Main plasma measurements made with the XUV spectrograph show that both intrinsic and puffed impurity levels in the plasma are doubled after detachment. Carbon levels in the main plasma are affected by either a change in the source or a change in the penetration efficiency. Measurements indicate that the source does not change after the detachment occurs, so that the change in carbon content of the plasma is primarily due to a change in the penetration efficiency. Similarly, for the recycling impurity neon, the source (constant gas puff) does not change upon detachment, but the neon content of the plasma does. This is indicated by the change in slope of the neon content versus time plot in Figure 7 (for a recycling impurity, the concentration is proportional to the integral of the source rate).[16] Similar results have been obtained when studying the argon gas puffed for core ion temperature measurements and other puffed impurity gases.

The neutral compression ratio is defined as the ratio of the neutral pressure in the divertor to the neutral pressure at the midplane. This parameter is important for maximizing pumping efficiency of deuterium and helium. High neutral densities in the divertor may also lead to better trapping of neutral impurities. Figure 8 shows that the compression ratio is reduced upon detachment of the divertor plasma. Under detached conditions the compression is reduced to a level equivalent to that of a non-dissipative divertor regime. This reduction is primarily due to an increase in the neutral pressure at the midplane as the divertor neutral pressure remains essentially constant. The increase in midplane pressure arises from a change in the ion flux profile on the divertor plates and a change in the leakage flux of neutrals around the divertor plates.[17] The ability to achieve high confinement modes may be hindered by this change in pressure because low neutral pressure on the midplane is believed to be an important parameter in the dynamics of H-modes.[18,19]

Probe measurements provide an independent estimate of the power lost from the plasma before it is convected and/or conducted to the divertor plates. In the high-recycling divertor the power that reaches the plates is low, typically about 20% of the total power input to the main plasma (see Figure 9). This power flux is measured with the embedded divertor probes and is calculated using $Q_{flux}^{div} = \gamma T_e J_{sat}$, where $\gamma$=7 is the sheath heat conduction factor, $T_e$ is the electron temperature, and $J_{sat}$ is the ion saturation current density. The resulting heat fluxes are integrated over the surface of the divertor plate to obtain the total power flowing to the divertor plates. This power flux to the plates is further reduced after the divertor plasma detaches, becoming $\leq$ 10% of the power input to the main plasma. In either type of dissipative divertor operation, the problem of removing the heat is eased, causing less erosion of the divertor plates. This is of course important for extending the lifetime of the divertor components in future tokamaks and reactors.

## VI. Conclusions

Alcator C-Mod operates routinely with a dissipative divertor. Operation in the high-recycling and detached divertor regimes has been demonstrated. For both ohmic and ICRF-heated discharges, the divertor is highly dissipative: $0.5 \times P_{SOL} \leq P_{rad}^{div} \leq 1.0 \times P_{SOL}$. This leads to low heat fluxes on the divertor plates. The corresponding volumetric loss emissivities are often $\geq 30$ MW-m$^{-3}$. These emissivities are approximately equal to those needed to radiate about 100 MW in the ITER divertor and thus bring the divertor heat load down to acceptable levels. In the high-recycling regime with the ion $\nabla B$ drift directed toward the divertor, the emissivity is peaked outside the LCFS near the inner divertor plates and along the outer leg of the separatrix. In the detached divertor regime, the emission peak is located inside the LCFS near the X-point. In ohmic plasmas, the radiating species in the divertor region have been identified. The most significant radiators are of low atomic number, namely carbon, oxygen, fluorine, and argon. Deuterium radiation, bremsstrahlung, and charge-exchange are also important loss channels in both dissipative divertor regimes.

The following advantages and disadvantages of detached divertor plasmas with respect to high-recycling divertor plasmas have been identified. There is less power radiated in the divertor region outside the LCFS relative to that radiated inside the LCFS. This is considered to be a disadvantage because the divertor volume is no longer being used effectively as a radiating region. The penetration efficiency of impurities, both intrinsic and puffed, is increased. This characteristic is unfavorable for the reason that the increase in main plasma impurities cools the core plasma and dilutes the fuel. The neutral compression ratio is reduced. A high compression ratio is favorable for pumping deuterium and helium and possibly indicative of a good impurity compression ratio. Lower neutral pressure at the midplane (high compression) also

appears to improve confinement and increase the upper density limit allowable for H-mode. The power flux to the divertor plates is reduced even further upon divertor detachment. This result clearly favors detached divertor operation in that the lifetime of the divertor components can be extended by the decrease in erosion and thermo-mechanical stresses.

Overall, it has been shown in Alcator C-Mod that dissipative divertor operation can be achieved with high divertor density ($n_e^{div} \sim 1 \times 10^{21}$ $m^{-3}$), high parallel power flux ($q_{||}^{SOL} \leq 0.5$ GW-$m^{-2}$), and a clean core plasma ( $Z_{eff} \leq 1.6$ ). This is possible with either high-recycling or detached divertor plasmas.

## Acknowledgements

Thanks to the Alcator C-Mod engineering and technical staffs for keeping all systems operational. A special thanks is extended to the computer gurus who maintain the Alcator C-Mod databases. This work is supported by the U.S. Department of Energy Contract # DE-AC02-78ET51013.

## References


[1]ITER - JCT ,"1995 ITER Design Description Document (WBS 1.9)," 1995.

[2]I.H. Hutchinson, R. Boivin, F. Bombarda, P. Bonoli, S. Fairfax, C. Fiore, J. Goetz, S. Golovato, R. Granetz, M. Greenwald, S. Horne, A. Hubbard, J. Irby, B. LaBombard, B. Lipschultz, E. Marmar, G. McCracken, M. Porkolab, J. Rice, J. Snipes, Y. Takase, J. Terry, S. Wolfe, C. Christensen, D. Garnier, M. Graf, T. Hsu, T. Luke, M. May, A. Niemczewski, G. Tinios, J. Schachter, and J. Urbahn, Physics of Plasmas, **1**, 1511 (1994).

[3]B. LaBombard, J. Goetz, C. Kurz, D. Jablonski, B. Lipschultz, G. McCracken, A. Niemczewski, R. L. Boivin, F. Bombarda, C. Christensen, S. Fairfax, C. Fiore, D. Garnier, M. Graf, S. Golovato, R. Granetz, M. Greenwald, S. Horne, A. Hubbard, I. Hutchinson, J. Irby, J. Kesner, T. Luke, E. Marmar, M. May, P. O'Shea, M. Porkolab, J. Reardon, J. Rice, J. Schachter, J. Snipes, P. Stek, Y. Takase, J. Terry, G. Tinios, R. Watterson, B. Welch, and S. Wolfe, Physics of Plasmas, **2**, 2242 (1995).

[4]G.F. Matthews, S.J. Fielding, G.M. McCracken, C.S. Pitcher, P.C. Stangeby, and M. Ulrickson, Plasma Physics and Controlled Fusion **32**, 1301 (1990).

[5]L.L. Lao, H. St. John, R.D. Stambaugh, A.G. Kellman, and W. Pfeiffer, Nuclear Fusion **25**, 1611 (1985).

[6]E.R. Müller, G. Weber, F. Mast, G. Schramm, E. Buchelt, and C. Andelfinger, "Design of a Four-channel Bolometer Module for ASDEX Upgrade and Tore Supra," Max-Planck-Institut für Plasmaphysik IPP Report 1/224 (1985).

[7]C. Kurz, J.A. Snipes, J.L. Terry, B. LaBombard, B. Lipschultz, and G.M. McCracken, Review of Scientific Instruments **66**, 619 (1995).

[8]A. Niemczewski, B. Lipschultz, B. LaBombard, and G. McCracken, Review of Scientific Instruments **66**, 360 (1995).

[9]B. LaBombard, D. Jablonski, B. Lipschultz, G. McCracken, and J. Goetz, Journal of

Nuclear Materials **220-222**, 976 (1995).

[10]P.C. Stangeby, Nuclear Fusion **33**, 1695 (1993).

[11]M. Greenwald, J. Terry, S. Wolfe, S. Ejima, M. Bell, S. Kaye, G.H. Neilsen, Nuclear Fusion **28** 12, 2199 (1988).

[12]B. Lipschultz, J.A. Goetz, I.H. Hutchinson, B. LaBombard, G.M. McCracken, A. Niemczewski, J.L. Terry, and S. Wolfe, in Proceedings of the 22nd European Physical Society Conference on Controlled Fusion and Plasma Physics, **19C-III**, 325 (1995).

[13]I.H. Hutchinson, B. LaBombard, J.A. Goetz, B. Lipschultz, G.M. McCracken, J.A. Snipes, and J.L. Terry, "The Effects of Field Reversal on the Alcator C-Mod Divertor," to appear in Plasma Physics and Controlled Fusion.

[14]J.L. Terry, J.A. Snipes, and C. Kurz, Review of Scientific Instruments **66**, 555 (1995).

[15]M.A. Graf, J.E. Rice, J.L. Terry, E.S. Marmar, J.A. Goetz, G.M. McCracken, F. Bombarda, and M.J. May, Review of Scientific Instruments **66**, 636 (1995).

[16]G.M. McCracken, B. Lipschultz, B. LaBombard, F. Bombarda, M. Graf, J.A. Goetz, R. Granetz, D. Jablonski, H. Ohkawa, J.E. Rice, J.L. Terry, Y. Wang, and B.L. Welch, in Proceedings of the 22nd European Physical Society Conference on Controlled Fusion and Plasma Physics, **19C-II**, 313 (1995).

[17]A. Niemczewski, B. Lipschultz, B. LaBombard, and G. McCracken, "Neutral Particle Dynamics in the Alcator C-Mod Tokamak," submitted to Nuclear Fusion (1995).

[18]ASDEX Team, Nuclear Fusion, **29**, 1959 (1989).

[19]J.A. Snipes, R.L. Boivin, C. Christensen, C. Fiore, D. Garnier, J.A.Goetz, S.N. Golovato, M. Graf, R.S. Granetz, M. Greenwald, A. Hubbard, I.H. Hutchinson, J. Irby, B. LaBombard, E.S. Marmar, A. Niemczewski, P. O'Shea, M. Porkolab, P. Stek, Y. Takase, J.L. Terry, M. Umansky, and S.M. Wolfe, "Characteristics of H-modes in Alcator C-Mod," submitted to Physics of Plasmas (1995).

**TABLE I**

Summary of Impurity Observations for Ohmic Plasmas

| radiated by | % of radiated XUV power for $\bar{n}_e^{main}$ ~ 1 x $10^{20}$ $m^{-3}$ | % of radiated XUV power for $\bar{n}_e^{main}$ ~ 2 x $10^{20}$ $m^{-3}$ |
|---|---|---|
| Ar | 19% | 11% |
| F | 13% | 13% |
| C | 10% | 9% |
| O | 9% | 13% |
| $D^0_{tot}$ | 6% | 20% |
| Bremsstrahlung | est.~3% | ~13% |
| N | 1% | <1% |
| He | <1% | <1% |
| Mo | <1% | <1% |
| unresolved lines | ~37% | ~18% |

**Figure Captions**

1. Schematic of the Alcator C-Mod divertor showing (a) the Langmuir probes and neutral pressure gauges and (b) the viewing chords of the bolometers used in this work. Also shown in (a) is the magnetic geometry used for these experiments.

2. Comparison of the electron pressure and temperature profiles "upstream" and at the divertor plate for the high-recycling and detached divertor regimes. The detached flux surfaces are indicated by the cross-hatching. Positive $\rho$ corresponds to the common flux zone.

3. Typical dissipative divertor conditions. The divertor plasma begins to detach at 0.62 sec, reattaches to the plates at 0.71 sec, and detaches again at 0.82 sec as indicated by the dotted lines. The initials HR signify the high-recycling regime and DD signify the detached divertor regime.

4. Emissivity contour plots in the divertor region. Volumetric emissivity in the (a) high-recycling and (b) detached divertor regime is obtained from bolometric tomography. The $D_\alpha$ emissivity (c) is obtained from $D_\alpha$ tomography. The contour plots correspond to (a) 0.6 sec and (b,c) 0.68 sec of the discharge depicted in Figure 3.

5. Comparison of bolometer brightness and total XUV brightness along a chord through the X-pt. The bolometer and XUV spectrograph viewing chords are nearly co-linear but separated toroidally. The total $D^0$ contribution is calculated from the brightness of the $D_{Ly\beta}$ line. Also shown is the typical central density and $Z_{eff}$ for this experiment.

6. Ratio of the power radiated in the divertor outside the LCFS to the total power radiated inside the LCFS versus the input power for dissipative divertor discharges. This ratio decreases when the divertor plasma detaches from the plates.

7. Brightness versus time of carbon, an intrinsic impurity, and neon, a puffed, recycling impurity. The central density versus time trace is also included for the two discharges

shown. The penetration efficiency of both impurities increases after divertor detachment.

8. Neutral compression ratio versus line-averaged central density for divertor discharges in Alcator C-Mod. There is a striking decrease in the neutral compression ratio after detachment.

9. Power flux to the divertor plates, $Q_{flux}^{div}$, versus input power for dissipative divertor discharges. The power flux is reduced from its already low value after detachment. Dashed lines indicating the 10% and 20% levels are included.

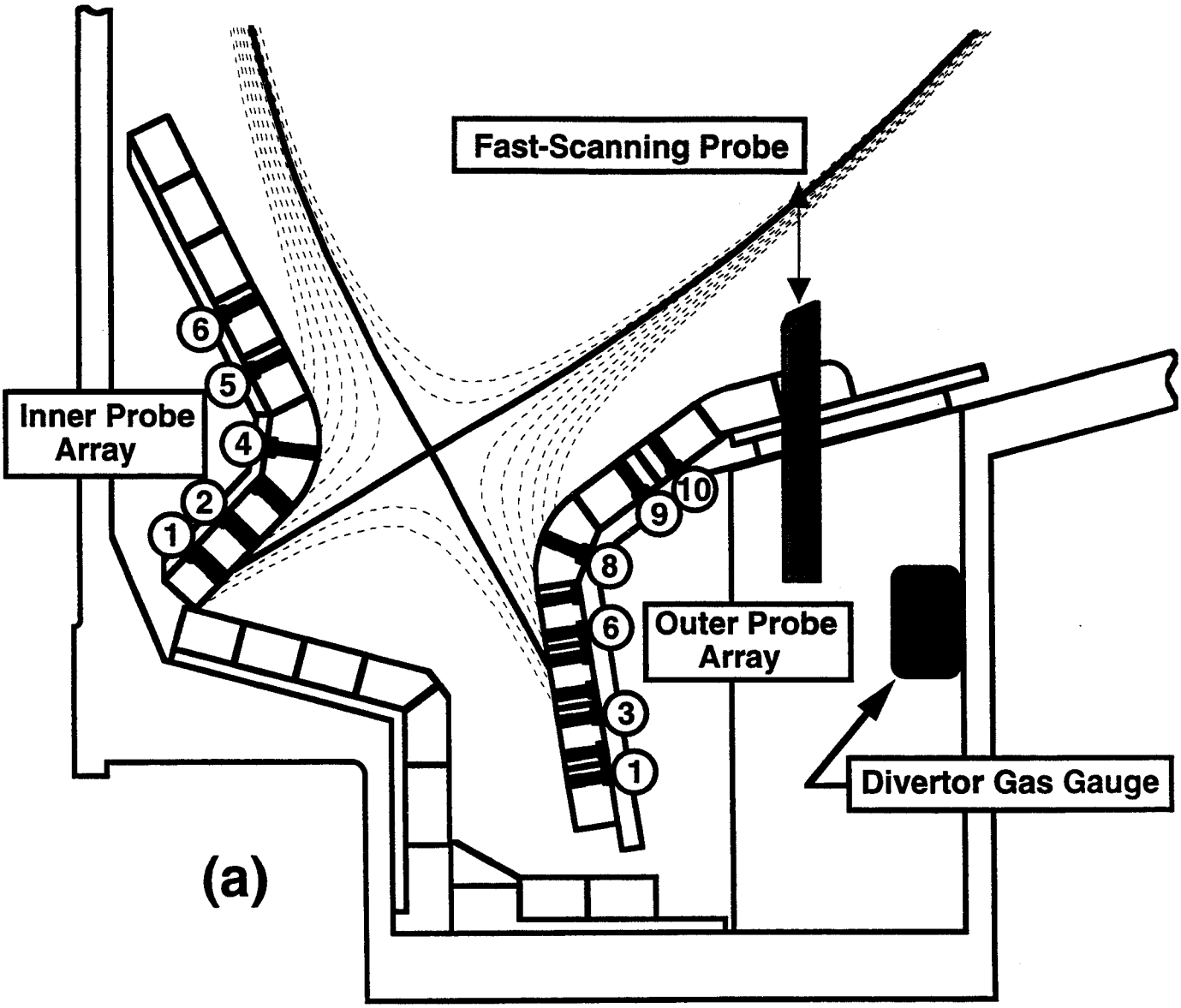
Fast-Scanning Probe
Inner Probe Array
Outer Probe Array
Divertor Gas Gauge
(a)
1
2
3
4
5
6
8
9
10

Figure 1(a)

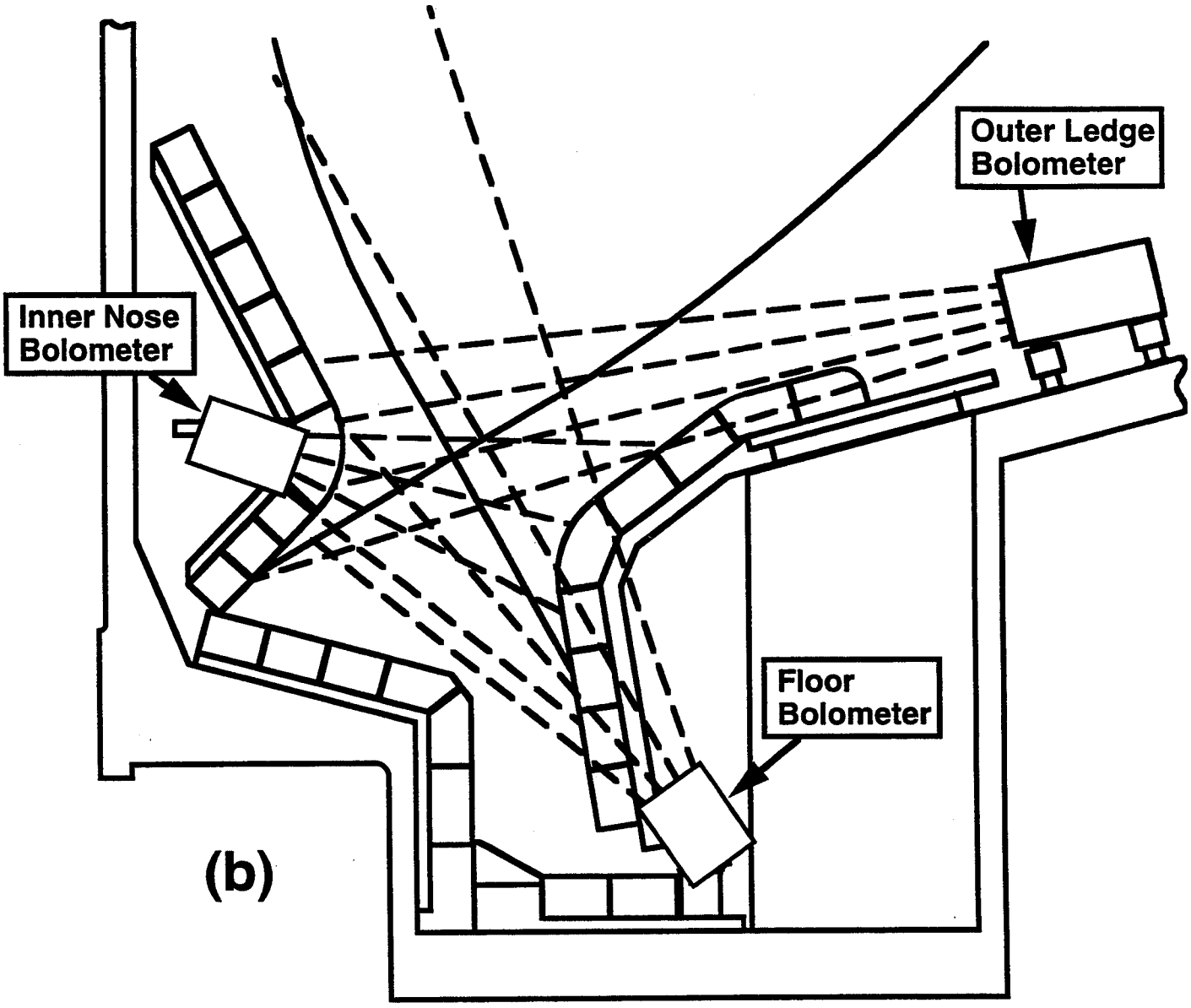
Outer Ledge
Bolometer
Inner Nose
Bolometer
Floor
Bolometer
(b)

Figure 1(b)

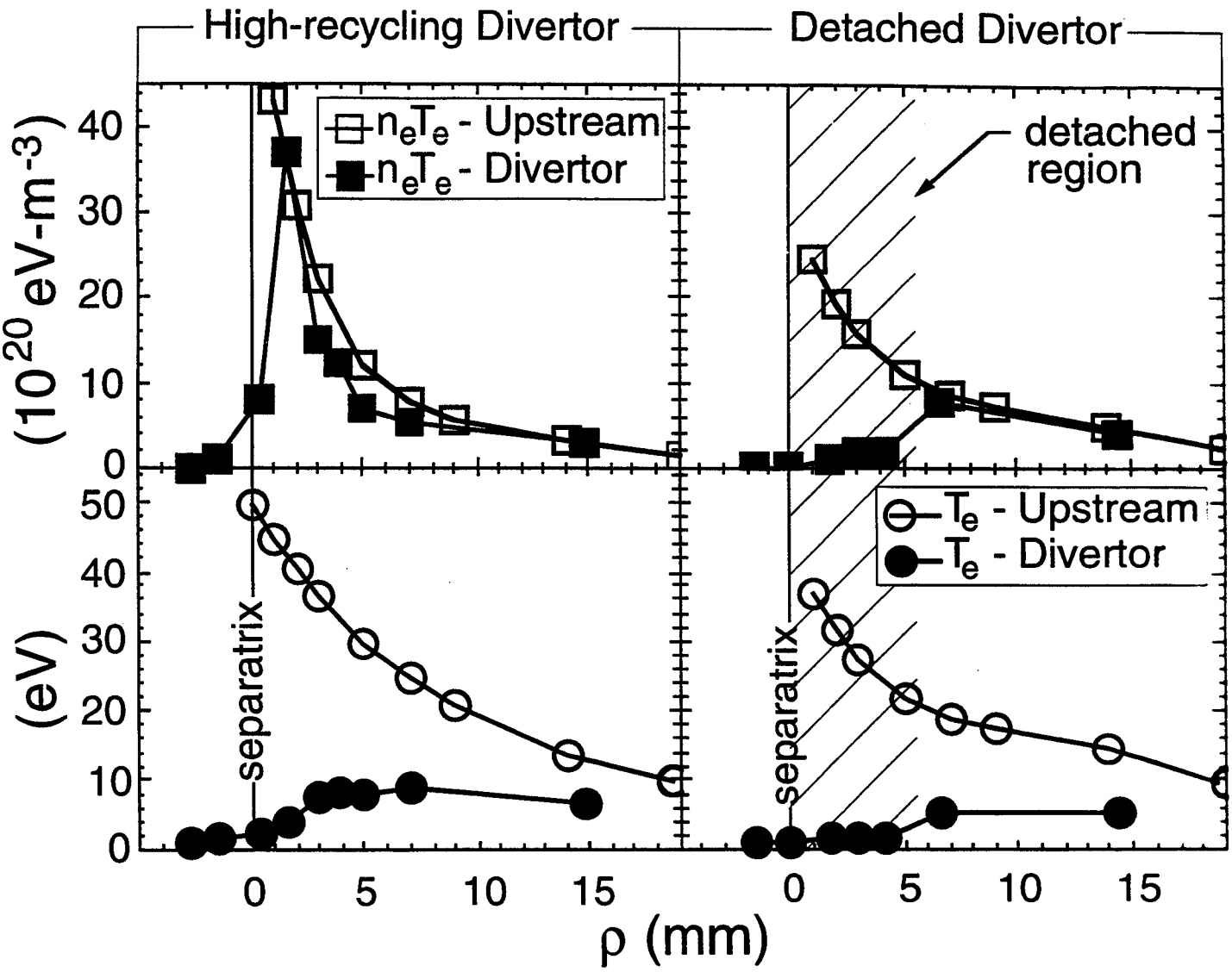
High-recycling Divertor
Detached Divertor
$n_eT_e$ - Upstream
$n_eT_e$ - Divertor
detached region
$(10^{20}$ eV-m$^{-3})$
$T_e$ - Upstream
$T_e$ - Divertor
separatrix
separatrix
(eV)
ρ (mm)

Figure 2

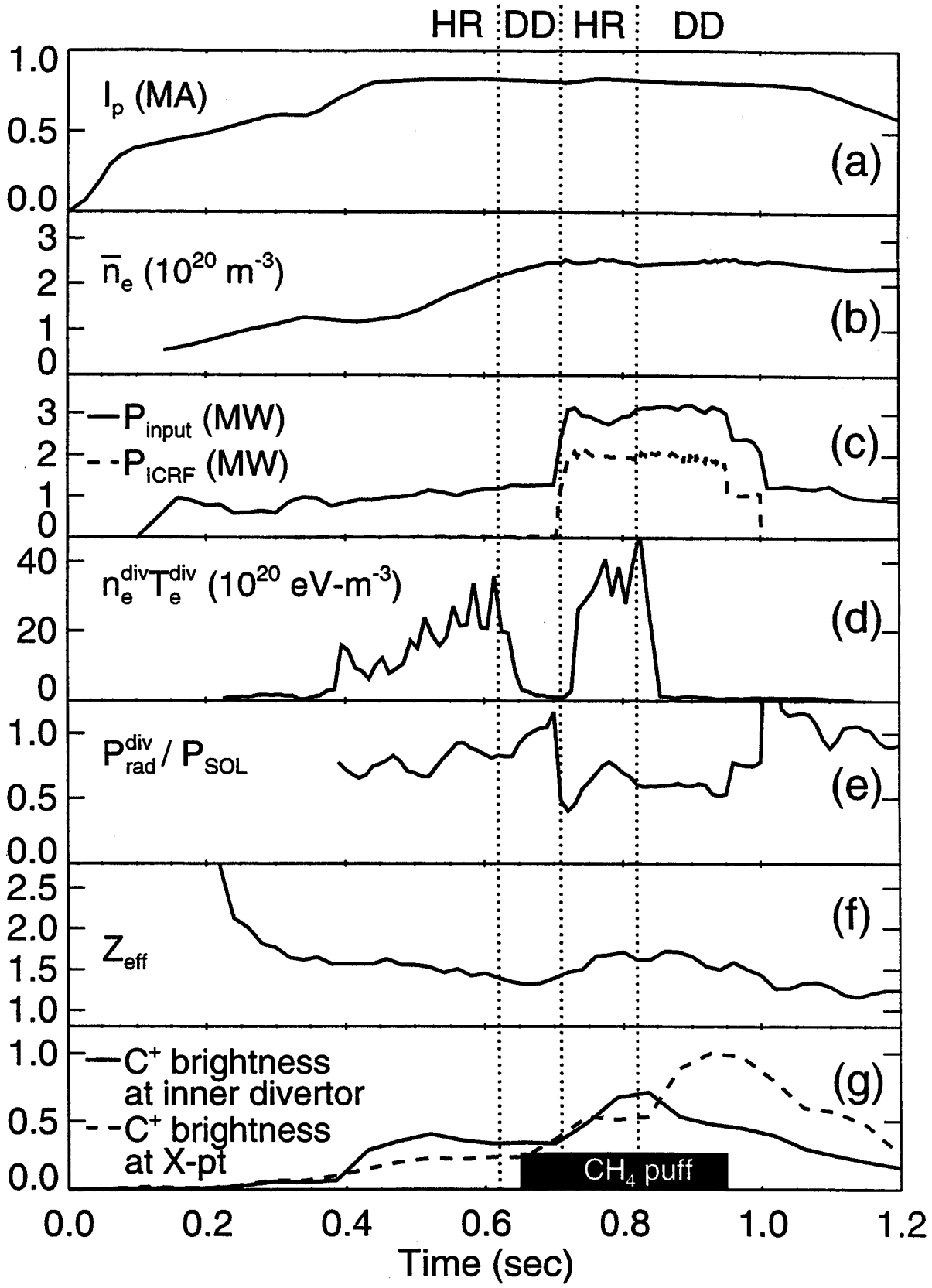
HR
DD
HR
DD
1.0
0.5
0.0
$I_p$ (MA)
(a)
3
2
1
0
$\bar{n}_e$ ($10^{20}$ m$^{-3}$)
(b)
3
2
1
0
—$P_{input}$ (MW)
- -$P_{ICRF}$ (MW)
(c)
40
20
0
$n_e^{div}T_e^{div}$ ($10^{20}$ eV-m$^{-3}$)
(d)
1.0
0.5
0.0
$P_{rad}^{div}$ / $P_{SOL}$
(e)
2.5
2.0
1.5
1.0
$Z_{eff}$
(f)
1.0
0.5
0.0
—$C^+$ brightness at inner divertor
- -$C^+$ brightness at X-pt
(g)
$CH_4$ puff
0.0
0.2
0.4
0.6
0.8
1.0
1.2
Time (sec)

Figure 3

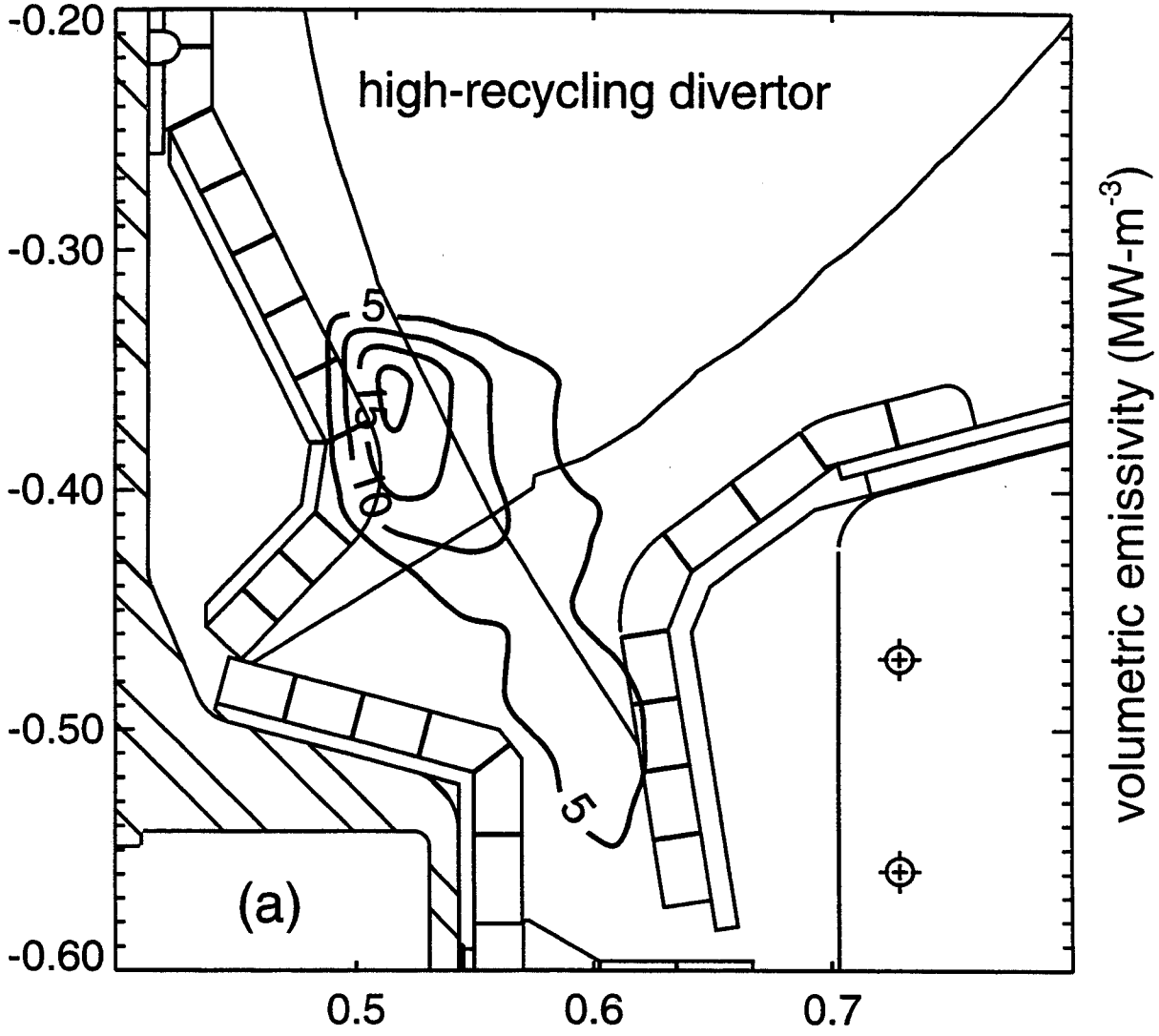
high-recycling divertor
(a)
-0.20
-0.30
-0.40
-0.50
-0.60
0.5
0.6
0.7
5
15
10
5
volumetric emissivity (MW-m-3)

Figure 4(a)

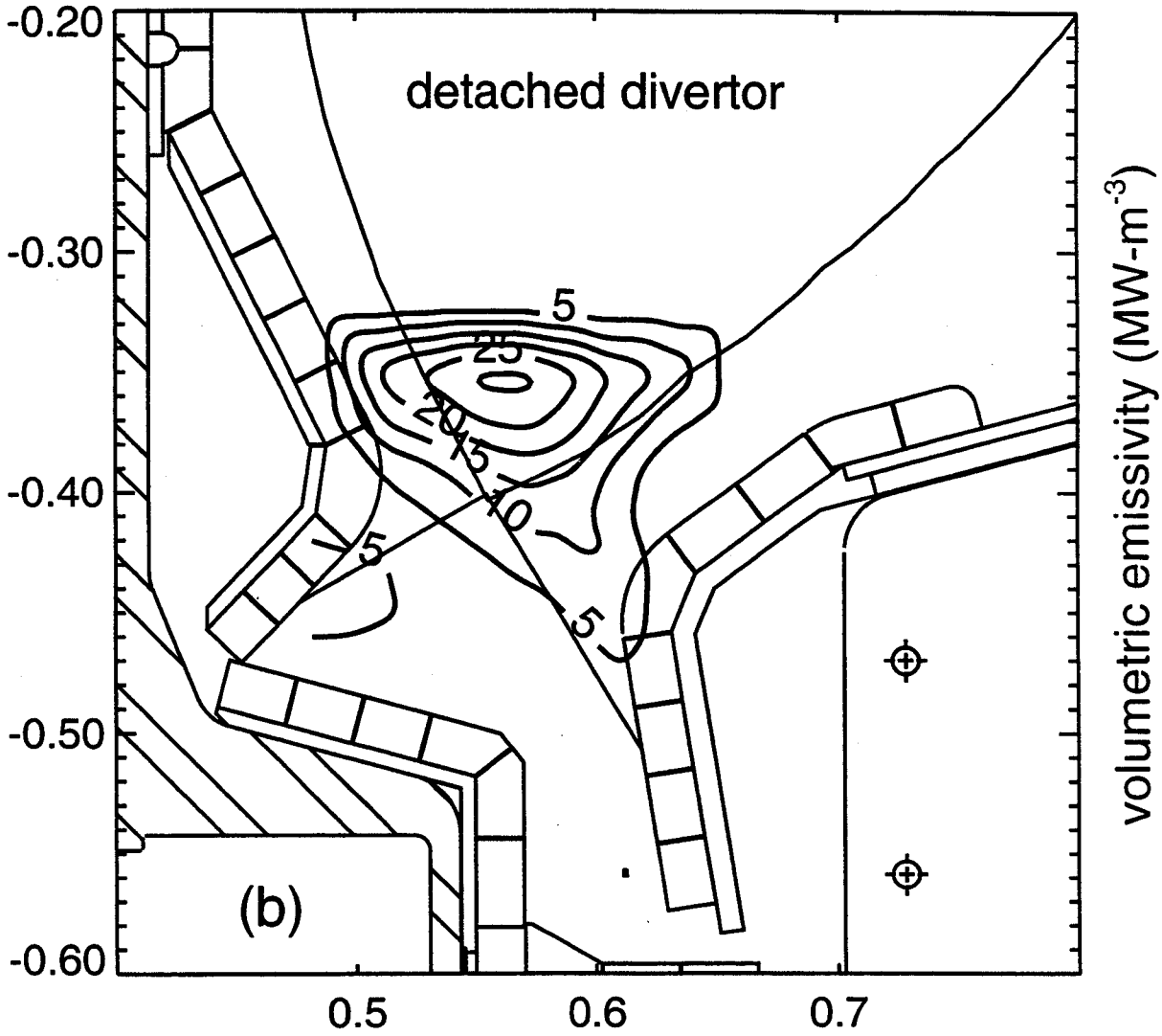
detached divertor
(b)
-0.20
-0.30
-0.40
-0.50
-0.60
0.5
0.6
0.7
5
25
20
15
10
5
5
volumetric emissivity (MW-m-3)

Figure 4(b)

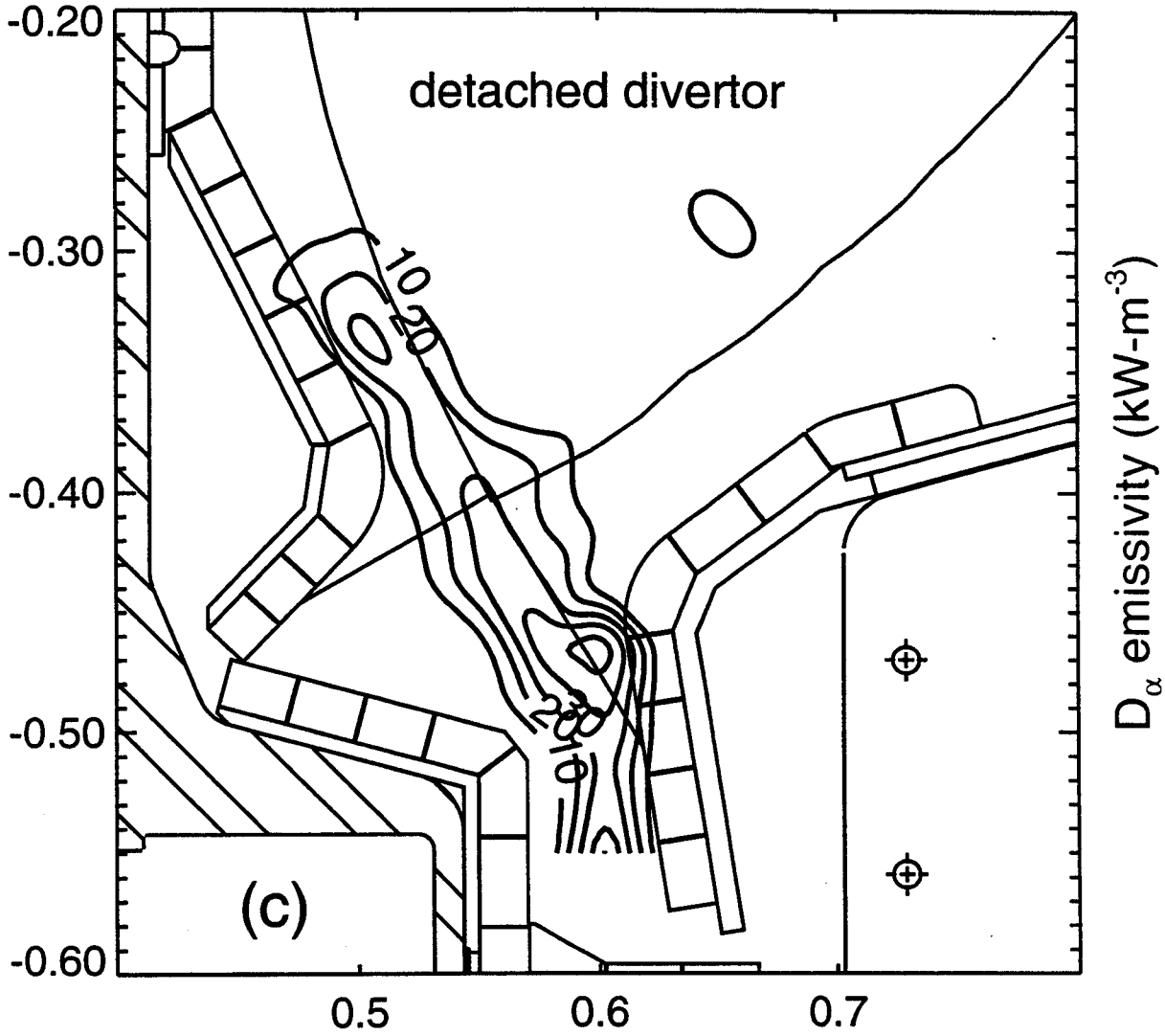
detached divertor
10
20
30
40
(c)
-0.20
-0.30
-0.40
-0.50
-0.60
0.5
0.6
0.7
$D_\alpha$ emissivity (kW-m$^{-3}$)

Figure 4(c)

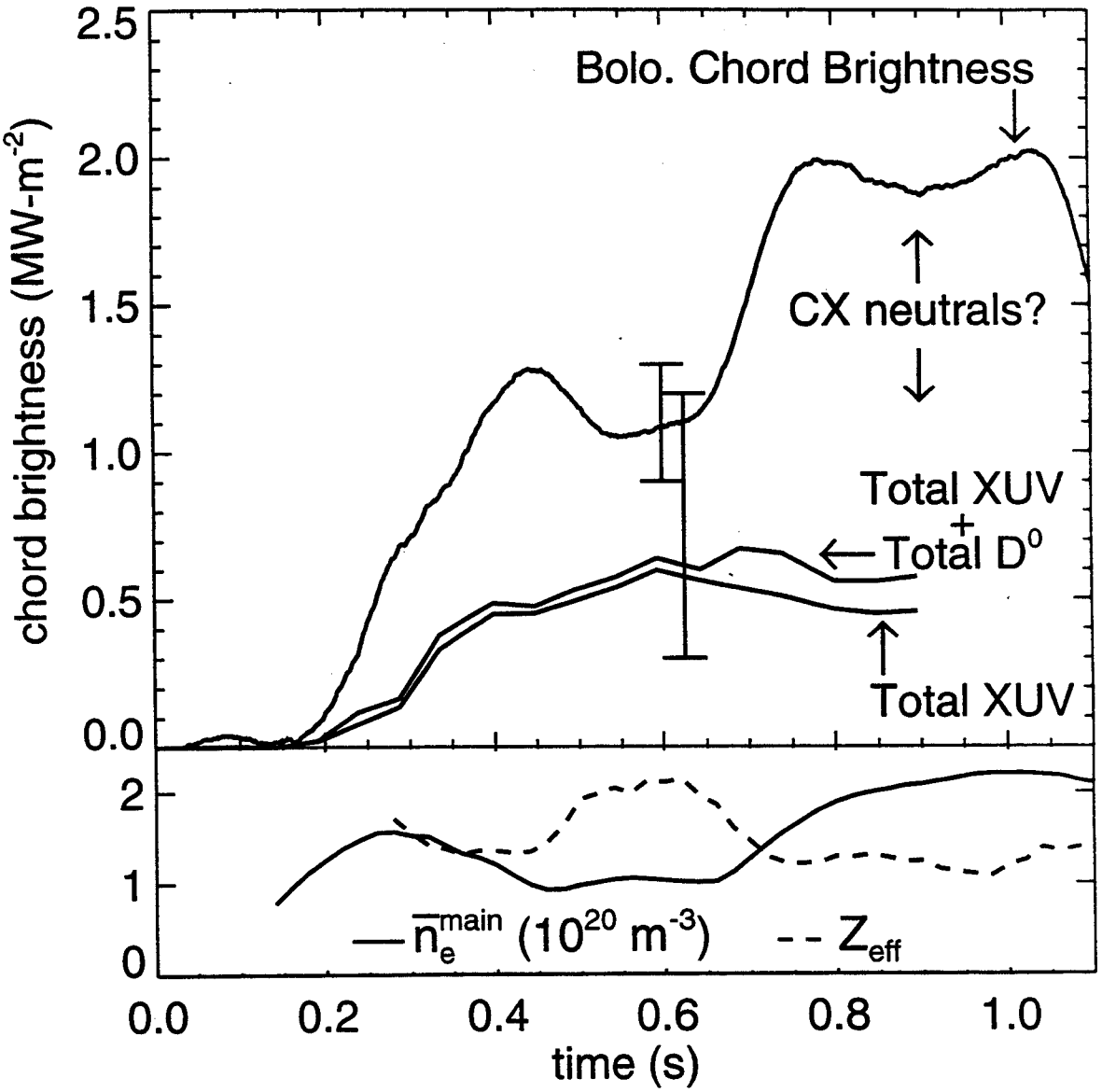
Bolo. Chord Brightness
CX neutrals?
Total XUV
+
Total D⁰
Total XUV
chord brightness (MW-m⁻²)
2.5
2.0
1.5
1.0
0.5
0.0
2
1
0
— $\bar{n}_e^{main}$ ($10^{20}$ m$^{-3}$)
-- $Z_{eff}$
0.0
0.2
0.4
0.6
0.8
1.0
time (s)

Figure 5

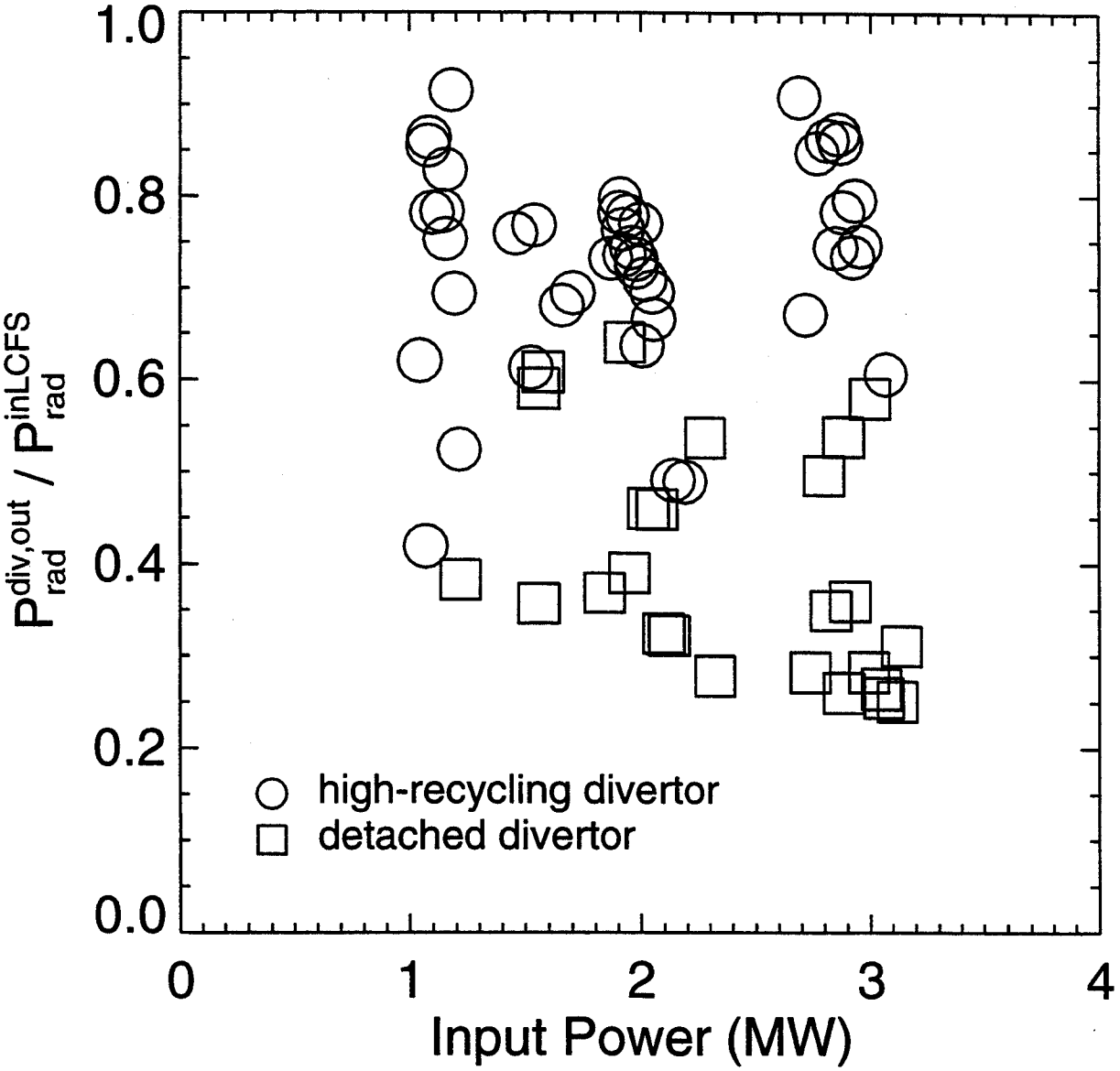
1.0
0.8
0.6
0.4
0.2
0.0
0
1
2
3
4
Input Power (MW)
$P_{rad}^{div,out} / P_{rad}^{inLCFS}$
high-recycling divertor
detached divertor

Figure 6

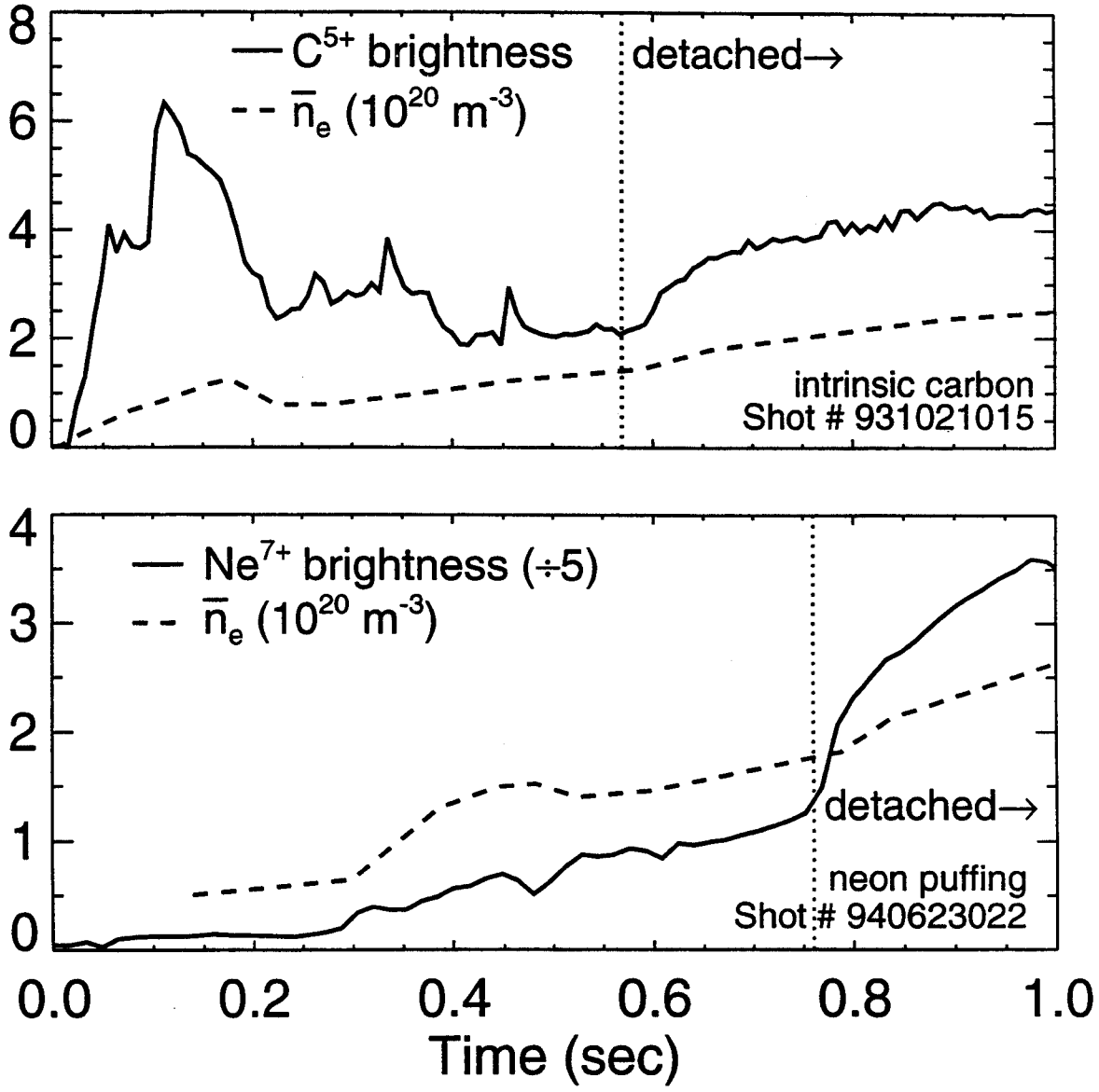
8
6
4
2
0
— $C^{5+}$ brightness
-- $\bar{n}_e$ ($10^{20}$ $m^{-3}$)
detached→
intrinsic carbon
Shot # 931021015
4
3
2
1
0
— $Ne^{7+}$ brightness (÷5)
-- $\bar{n}_e$ ($10^{20}$ $m^{-3}$)
detached→
neon puffing
Shot # 940623022
0.0
0.2
0.4
0.6
0.8
1.0
Time (sec)

Figure 7

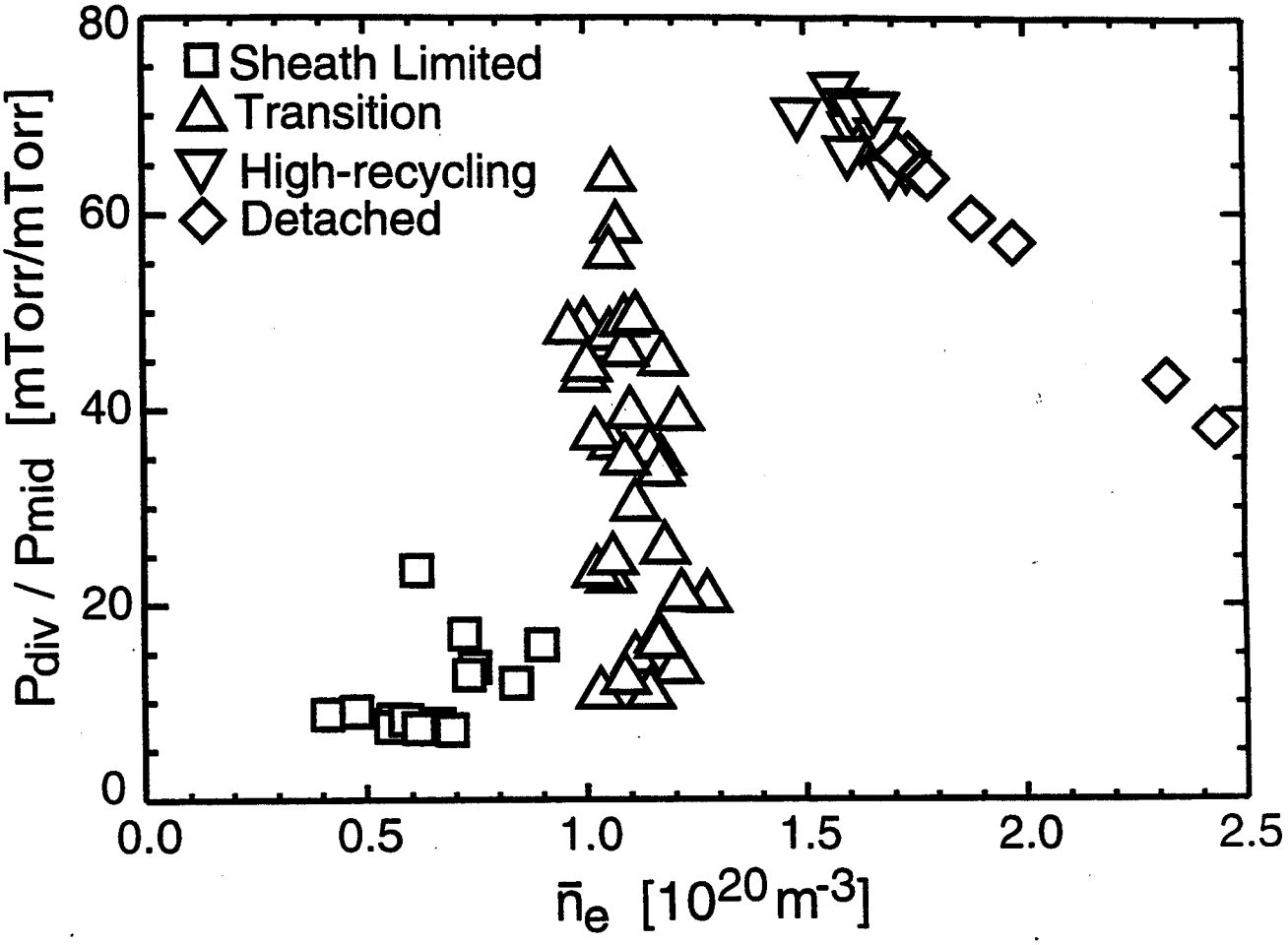
Sheath Limited
Transition
High-recycling
Detached
$P_{div}$ / Pmid [mTorr/mTorr]
$\bar{n}_e$ [$10^{20}$ $m^{-3}$]
0
20
40
60
80
0.0
0.5
1.0
1.5
2.0
2.5

Figure 8

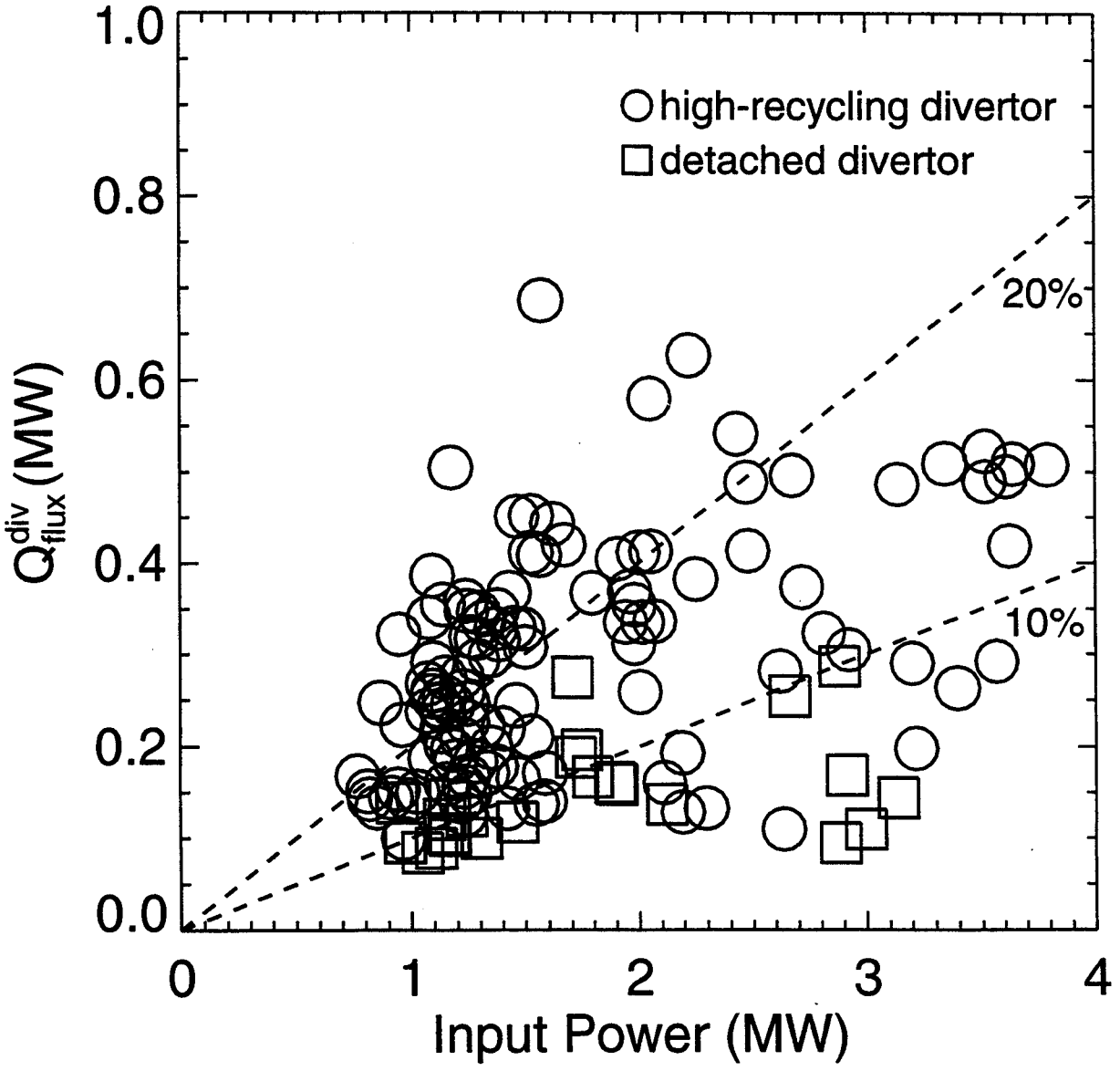
1.0
0.8
0.6
0.4
0.2
0.0
0
1
2
3
4
Input Power (MW)
$Q_{flux}^{div}$ (MW)
high-recycling divertor
detached divertor
20%
10%

Figure 9